Research on the model of high robustness computational optical imaging system

Yun Su(苏云)[1,2], Teli Xi(席特立)[1], and Xiaopeng Shao(邵晓鹏)[1,†]

[1] *School of Optoelectronic Engineering, Xidian University, Xi'an* 710071, *China*
[2] *Beijing Institute of Space Mechanics & Electricity, Beijing* 100094, *China*

(Received 19 June 2022; revised manuscript received 22 September 2022; accepted manuscript online 19 October 2022)

Computational optical imaging is an interdisciplinary subject integrating optics, mathematics, and information technology. It introduces information processing into optical imaging and combines it with intelligent computing, subverting the imaging mechanism of traditional optical imaging which only relies on orderly information transmission. To meet the high-precision requirements of traditional optical imaging for optical processing and adjustment, as well as to solve its problems of being sensitive to gravity and temperature in use, we establish an optical imaging system model from the perspective of computational optical imaging and studies how to design and solve the imaging consistency problem of optical system under the influence of gravity, thermal effect, stress, and other external environment to build a high robustness optical system. The results show that the high robustness interval of the optical system exists and can effectively reduce the sensitivity of the optical system to the disturbance of each link, thus realizing the high robustness of optical imaging.

Keywords: computational optical imaging, high robustness, sensitivity

PACS: 42.15.Eq, 42.82.Bq, 42.88.+h, 42.30.Kq **DOI:** 10.1088/1674-1056/ac9b34

1. Introduction

With the continuous expansion of human cognitive boundaries, optical systems as an important means of human perception of the world, its imaging needs are also increasing. In the pursuit of higher imaging performance, system stability has become one of the problems that must be faced.

Any optical system will be affected by the thermal and force factors in the process of machining,[1–3] installation, adjustment, or operation, which will produce maladjustment, that is, the tolerance problem in optical engineering.[4,5] Moreover, because the optical wavelength is relatively short, generally in the order of 100 nanometers, the traditional design method requires the tolerance of the optical system to be comparable to its wavelength. Therefore, the optical system in the process of engineering implementation requires not only extremely high precision of machining, installation, and adjustment but also a high level of gravity unloading and temperature control, which brings great challenges to the implementation and reliable operation of the optical system.

Because of the reliability of the system, based on the theory of system fault-tolerant control, it is generally possible to reduce the influence of system errors caused by environmental factors through active fault tolerance (active FTC) and passive fault tolerance (passive FTC).[6]

Traditional active fault-tolerant control systems diagnose faults by observing the occurrence of faults and feeding the fault information to the controller for adjustment, to realize the error correction of the system. Although active FTC has high performance in fault identification and correction, the complexity of the control algorithm is increased as well as the delay of the system due to the three steps of fault observation, feedback and adjustment. Existing active fault-tolerant control systems mainly rely on known prior information, and improve the performance of the control system by designing high-performance control algorithms to shorten the time cost of fault diagnosis and improve the response time and accuracy of the controller as much as possible.

Passive FTC refers to the design of a control system to make it robust to specific faults without relying on fault feedback and changing the overall system structure. Therefore, compared with the active control, the passive fault-tolerant control reduces the fault observation, feedback, and compensation links, and has better timeliness and lower system complexity. Its disadvantage is that the adaptive ability of fault tolerance is very limited, and it cannot tolerate unknown fault conditions.

Computational imaging as a multidisciplinary cross frontier of new imaging technology, integrating optics, mathematics, and information technology, by the information transmission. This technique pays attention to the whole link integration global optimization design and introduce the main passive information coding and numerical calculation, change traditional imaging "what you see is what you get" mode of imaging, using numerical decoding for target imaging information. In the process of an optical imaging system, gravity, temperature and other factors will affect the information recorded by the system. Therefore, through the combination of computational imaging theory and passive fault-tolerant control, the

†Corresponding author. E-mail: xpshao@xidian.edu.cn

© 2023 Chinese Physical Society and IOP Publishing Ltd

robust control idea is introduced in the process of information coding to ensure the consistency of information transmission under different working conditions. In this manuscript, we do not pursue the minimum aberration of the optical system itself but focus on the imaging consistency after the influence of the external environment such as gravity, thermal effect, and stress on the optical system. To ensure that the imaging effect of the optical system is consistent under different working conditions, to facilitate the reconstruction and reprocessing of the image in the later stage.

2. High robustness of computational optical imaging model theory

The model of a non-ideal mirror participating in the imaging process can be equivalent to the superposition of the ideal mirror and error. The aberration-free pupil function is defined as

$$P(\xi,\eta)=\begin{cases}1, & \text{inside pupil},\\ 0, & \text{outside pupil}.\end{cases} \tag{1}$$

The error of each link of the optical system is equivalent to superimposing a phase difference function with certain randomness on the ideal pupil function, and its mathematical expression is

$$P(\xi,\eta)=\begin{cases}\exp[\mathrm{j}kW_{\text{random}}], & \text{inside pupil},\\ 0, & \text{outside pupil},\end{cases} \tag{2}$$

where W_{random} can be understood as the equivalent phase modulation on the pupil plane during all kinds of aberrations involved in the imaging of the optical system. Furthermore, in the actual optical imaging process, W_{random} can also be simply understood as the deformation of the primary mirror caused by its processing, assembly, gravity deformation, and thermal deformation, and the additional phase difference introduced by the optical system caused by this deformation. The frequency domain expression H of the point impact response function h of the optical system is

$$H\left(f_\xi,f_\eta\right)=\frac{\iint_{-\infty}^{+\infty}P(\xi,\eta)P\left(\xi+\lambda\,\mathrm{d}f_\xi,\eta+\lambda\,\mathrm{d}f_\eta\right)\mathrm{d}\xi\,\mathrm{d}\eta}{\iint_{-\infty}^{+\infty}P(\xi,\eta)\mathrm{d}\xi\,\mathrm{d}\eta}. \tag{3}$$

A highly robust computational optical imaging system model is shown in Fig. 1. In the figure, o is an external input signal, which generally refers to the scene; i is a controlled output, usually an image output with degraded imaging; h is the optical imaging system, that is, the point impact response of the optical system; u is a measurement output, which may be a sensor output and command signal, and v is a feedback control signal. H and K are frequency representations of generalized controlled devices and controllers, and it is assumed that the transfer function matrices $\boldsymbol{H}(s)$ and $\boldsymbol{K}(s)$ are real rational function matrices.

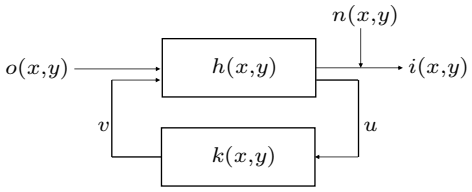


Fig. 1. Imaging model with high robustness for optical system imaging.

The optical system h is in an unstable state due to W_{random}, and the input image o changes because of this instability. Therefore, it is necessary to solve the appropriate controller k to effectively compensate for the instability of h and ensure the stability of the input image o.

The optical system optimized by the fault-tolerant controller has better fault-tolerant characteristics.[6] Active fault-tolerant control is to generate compensation signal v by measuring signal u, so as to ensure the stability of h. And the passive fault-tolerant control method needs to optimize the design of a specific constant k to ensure the stability of the input image o. This is also the key problem to be solved by the high robustness computational optical system. According to the H_∞ control theory,[7] the standard problem is to find a real and rational controller k to make h stable and make the H_∞ norm of the transfer function matrix $\boldsymbol{F}(\boldsymbol{H},\boldsymbol{K})$ infinitesimal, namely,

$$\min\|\boldsymbol{F}_i(\boldsymbol{H},\boldsymbol{K})\|_\infty. \tag{4}$$

The optical system design is guided by fault-tolerant control. In order to achieve high robustness of the computational optical system, the traditional optical design results are taken as the initial value. On the basis of this initial value, on the one hand, the multi-form disturbance is added to the optical system; on the other hand, by setting optical elements as controllers in the optical path and taking the stability of the optical system under the multi-form disturbance as the new objective function, the robust solution interval of the optical system can finally be reached.

3. Robustness model solution for computational optical systems

3.1. Optical system and disturbance modeling

Take a large aperture optical imaging system as a model, and its index is shown in Table 1.

Table 1. Design index of a large aperture optical imaging system.

No.	Items	Index
1	working spectrum	0.50 μm–0.80 μm
2	entrance pupil diameter	2.5 m
3	focal length	21.6 m
4	FOV	$0.65^\circ\times0.18^\circ$
5	pixel size	6 μm
6	MTF@83.3 lp/mm	≥ 0.33

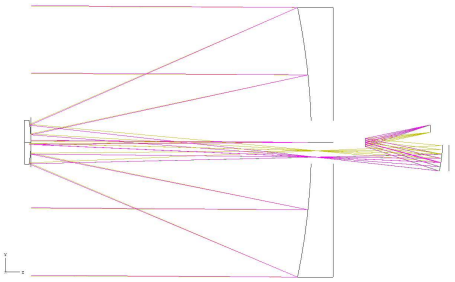


Fig. 2. Optical path of a large aperture optical imaging system.

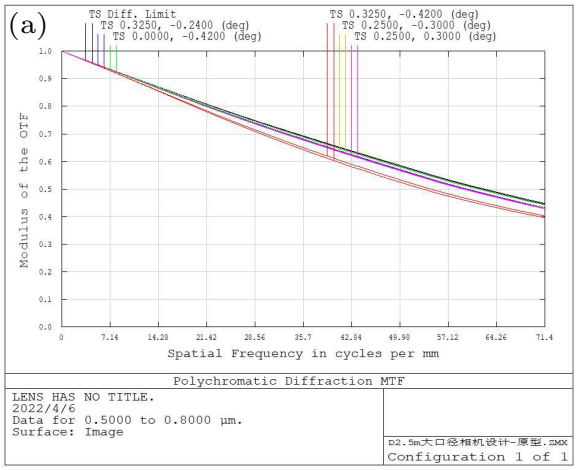


Fig. 3. Optical performance parameters of large aperture optical system: (a) MTF curve, (b) point spread function.

Taking this index as input, the optical system design result obtained by using the optimization method is shown in Fig. 2.

In order to visually express the imaging performance of the optical system under ideal conditions, the imaging performance parameters of the optical system are shown in the Fig. 3.

As can be seen from Fig. 3(a), the horizontal and vertical resolution distribution of the large aperture optical system designed according to the parameters in Table 1 is relatively consistent, and the edge resolution is about 50% lower than the center of the system, which is consistent with the same type of system. It can also be seen from the PSF image of the system that the energy of the system is concentrated and meets the imaging requirements. In a practical application, the supporting mode of the optical–mechanical system and the thermal effect are the main reasons that affect the imaging quality of the large-aperture optical system. Taking the large-aperture optical system designed with the parameters in Table 1 as an example, the thermal effect will be analyzed with finite element software.[8,9]

3.1.1. Modeling analysis of optomechanical thermal mode

Considering the large diameter of the primary mirror, two supporting schemes of 3-point and 6-point are designed. The specific modeling process is not detailed in this paper. The finite element models of the completed camera and its primary mirror are exhibited in Fig. 4.

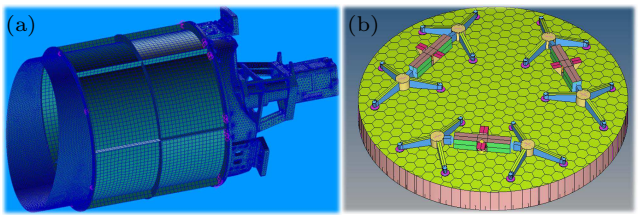


Fig. 4. Finite element modeling of a large aperture optical system: (a) the whole camera, (b) the primary mirror.

According to the finite element model of the camera, considering the support mode of the primary mirror, it provides a reference for us to set the disturbance of the primary mirror in different scenes.

3.1.2. Disturbance condition setting

Based on the thermal and structural design, the deformation characteristics of the primary mirror under typical working conditions in orbit are obtained through the optical-mechanical thermal integrated analysis,[10] as shown in Table 2 and Fig. 5. The deformation error distribution of the primary mirror at 0.1λ was studied under the conditions of three-point support weightlessness deformation, radial linear temperature gradient deformation, six-point support weightlessness deformation, and radial annular temperature gradient deformation of the primary mirror. And it is compared with

Table 2. Typical mechanical and thermal working conditions.

Working condition	Description	Primary mirror RMS
1	ideal condition	no quoted error
2	three-point support weightlessness deformation of the primary mirror	0.1 wavelength
3	radial linear temperature gradient deformation	0.1 wavelength
4	six-point support weightlessness deformation	0.1 wavelength
5	radial annular temperature gradient deformation	0.1 wavelength

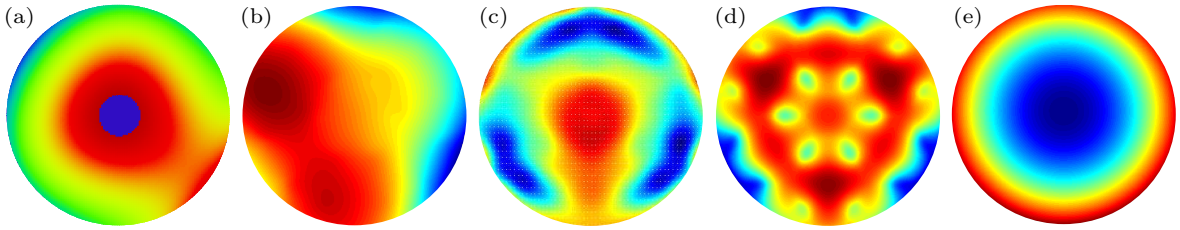


Fig. 5. Deformation error distribution of the primary mirror: (a) the ideal working condition, (b) the three-point support weightlessness deformation, (c) radial linear temperature gradient deformation, (d) six-point support weightlessness deformation, (e) radial annular temperature gradient deformation.

the ideal working condition. From the simulation results in Table 2, it can be seen that the deformation error of the primary mirror caused by the difference between support points and temperature gradients is also very different, and there is no obvious rule.

3.1.3. Instability analysis of the optical system under multiple working conditions

The distortion of the pupil surface is added to the optical simulation software so that the disturbance input of various error sources is completed. The detailed mirror error analysis methods are as follows:

(i) Analyze the surface shape quality of the mirror by using the finite element method, and the deformed surface is obtained.

(ii) Sample on the surface of the mirror to obtain the deformation values ($\mathrm{d}x_i$, $\mathrm{d}y_i$, and $\mathrm{d}z_i$) of the sampling points.

(iii) The deformation data is processed, that is, the deformation results in the Cartesian coordinate system (spherical coordinate system or cylindrical coordinate system) calculated by finite element program are converted into the data form in the sagittal direction or surface normal direction acceptable to optical analysis software.

As shown in the figure below, assuming that there is a point Z_0 on the mirror before deformation, after deformation it is Z_0'. And the point before deformation corresponding to Z_0' in the sagittal direction is Z_1, then under the action of small disturbance ($\mathrm{d}x$, $\mathrm{d}y$, and $\mathrm{d}z$), the deformation in the sag direction ($\mathrm{d}s$) can be calculated as follows: $\mathrm{d}s = \Delta z - (z_1 - z_0)$, where the values of z_1 and z_0 can be obtained by the curved surface equation.

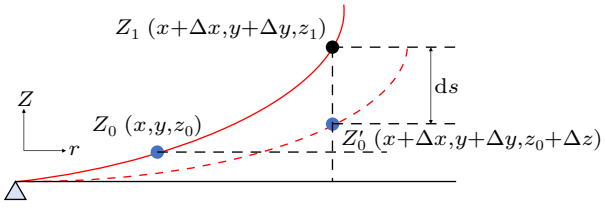


Fig. 6. Z-direction deformation and sagittal deformation of finite element analysis.[11]

(iv) Error fitting with Zernike polynomial

After the position error of the mirror is removed, the residual error of the mirror is fitted by Zernike polynomial.[12,13] The continuous wavefront in the unit pupil can be expressed as a linear combination of Zernike (circular or annular region) polynomials:

$$w(x,y,\varepsilon) = \sum_{j=1}^{L} a_j U(j,x,y,\varepsilon), \tag{5}$$

where $w(x,y,\varepsilon)$ is a continuous wave surface function; $U(j,x,y,\varepsilon)$ is the j Zernike polynomial in a rectangular coordinate system; L is the total number of fitting terms; a_j is the coefficient of the Zernike polynomial of the j-th term. It is assumed that the fitted wave surface consists of N discrete sampling points $S(x_i,y_i)$, $i = 1,2,\ldots,N$, and the least square condition of its fitting with the wave surface function can be expressed as

$$\Delta = \sum_{i=1}^{N} [a_j U(j,x_i,y_i,\varepsilon) - S(x_i,y_i)]^2 \to \min. \tag{6}$$

The formula above can be written in a matrix form:[14] $\boldsymbol{U}\boldsymbol{a} = \boldsymbol{S}$.

After solving the coefficient vector $\boldsymbol{a}$, Zernike polynomial can be used to describe the imaging wave surface of the optical system.[15]

It is used as the aberration input of the pupil position of the optical system through data acquisition and data preprocessing. The image quality degradation will happen in different degrees due to simulated aberration. MTF and PSF are mainly used to evaluate the image quality degradation of the optical system after the error is introduced, as shown in Fig. 7 (here, different configurations are used to express the errors in different states).

Four different types of error terms are applied to the pupil of the optical system, and the RMS error values of the surface shape are all 0.1. Compared with the PSF of the system without aberration, the PSF image is seriously degraded, and the energy dissipates seriously at the focal plane due to the introduction of the error term. Comparing the MTF curves of the system under different error conditions, the error makes the MTF curve at the edge drop obviously, which seriously affects the application of the large aperture optical system in practice.

In order to evaluate the effectiveness of the design method proposed in this paper, structural similarity (SSIM) is introduced to evaluate the consistency of the system PSF before and after robustness optimization. We perform imaging simulation on the original optical system without high robustness design, as shown in Fig. 8.

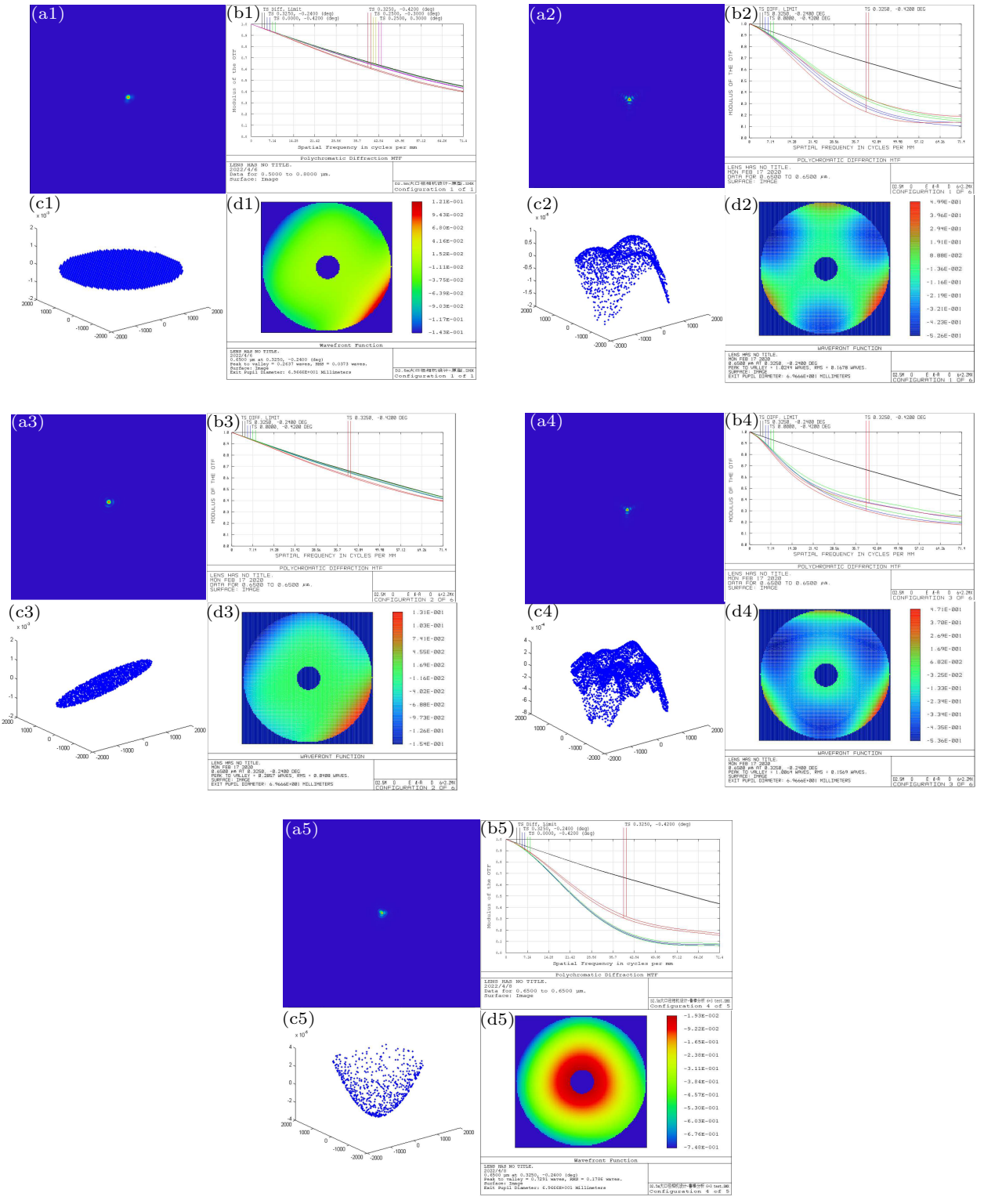


Fig. 7. Analysis of optical system maladjustment under typical mechanical and thermal conditions from configuration (config) 1 to configuration (config) 5. Panels (a1)–(a5) show PSF at the best focal plane, panels (b1)–(b5) show MTF at the best focal plane, panels (c1)–(c5) show error term form at pupil position, and panels (d1)–(d5) show wavefront diagram at the best focal plane.

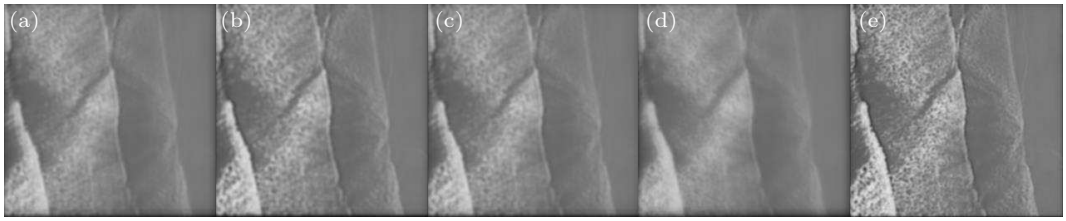


Fig. 8. Imaging simulation results of the original optical system from config 1–config 5.

Table 3. Comparison of imaging simulation results from config 1–config 5 by using SSIM.

Config	a	b	c	d	e
a	1	*	*	*	*
b	0.7931	1	*	*	*
c	0.8271	0.9533	1	*	*
d	0.8062	0.9937	0.9244	1	*
e	0.7555	0.9672	0.9024	0.9534	1

Note: * represents duplicate data.

It can be seen that under the influence of different configuration conditions, the imaging quality of the system also changes to different degrees. And we use SSIM to calculate and compare the similarity of imaging simulation results from config 1–config 5, as shown in Table 3.

It can be seen that the imaging simulation results of the system under the influence of different configuration conditions have certain differences, indicating that the environmental interference will have different degrees of impact on the imaging quality of the optical system.

3.2. Robust interval and pupil initial value solutions

3.2.1. Robust interval initial value solution

Generally, aberration is equivalent to pupil function superimposed with different wave aberration functions for the optical system.

For the space camera in orbit, the degradation of the system imaging quality caused by gravity or temperature changes is equivalent to the change of the wave aberration function of the pupil surface of the optical system itself. Assuming that the wave aberration is $W_1(\xi,\eta),\ldots,W_N(\xi,\eta)$ under N different working conditions, then

$$P_1 = \begin{cases} \exp[\mathrm{j}kW_1(\xi,\eta)], & \text{inside pupil,} \\ 0, & \text{outside pupil,} \end{cases} \tag{7}$$

$$P_2 = \begin{cases} \exp[\mathrm{j}kW_2(\xi,\eta)], & \text{inside pupil,} \\ 0, & \text{outside pupil,} \end{cases} \tag{8}$$

$$\vdots$$

$$P_N = \begin{cases} \exp[\mathrm{j}kW_N(\xi,\eta)], & \text{inside pupil,} \\ 0, & \text{outside pupil.} \end{cases} \tag{9}$$

Assuming that an active modulation wave aberration Z can be superimposed on the pupil function by an active modulation optical system. The imaging process of that optical system can be expressed as follows:

$$o \otimes p \otimes z = i. \tag{10}$$

Here o is the spatial domain representation of objects, p is the spatial domain representation of pupil function, z is the spatial domain representation of superimposed wave aberration, and i is the spatial domain representation of images.

Fourier transform is performed on the above imaging process to obtain its frequency domain representation as follows:

$$\mathcal{F}(o \otimes p \otimes z = i) = \mathcal{F}(i), \tag{11}$$

that is,

$$O \cdot P \cdot Z = I, \tag{12}$$

so,

$$P \cdot Z = I/O, \tag{13}$$

demand that,

$$I/O = C, \tag{14}$$

C represents the degradation parameters of images and objects, and it needs to be controlled in a certain acceptable range.

Because of the disturbance caused by different wave aberrations, it is necessary to maintain the robustness of C through the actively superimposed wave aberration Z, which can be modeled by the least square method as follows:

$$\begin{bmatrix} P_1 \\ P_2 \\ \vdots \\ P_N \end{bmatrix} \cdot Z = C. \tag{15}$$

The initial value of the wave aberration z can be obtained by the least square solution.

The initial value z of WFE is obtained by the above method, but it cannot be directly used in the optimal design of the system. Instead, the z value should be converted into the modulation parameter of the exit pupil plane of the optical system.

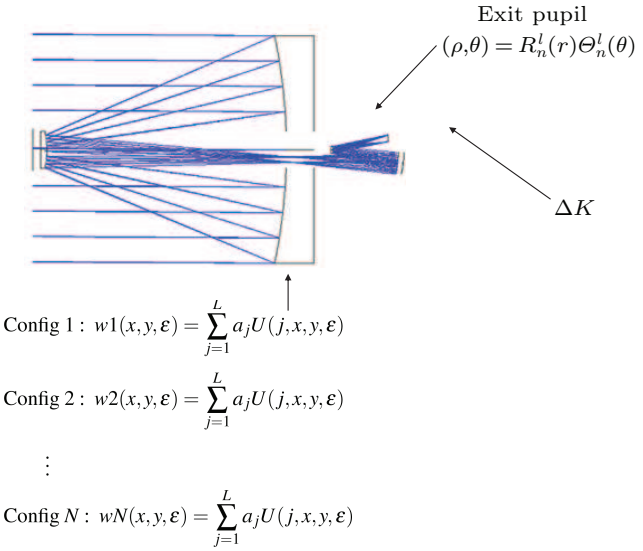


Fig. 9. High robustness design of optical imaging system.

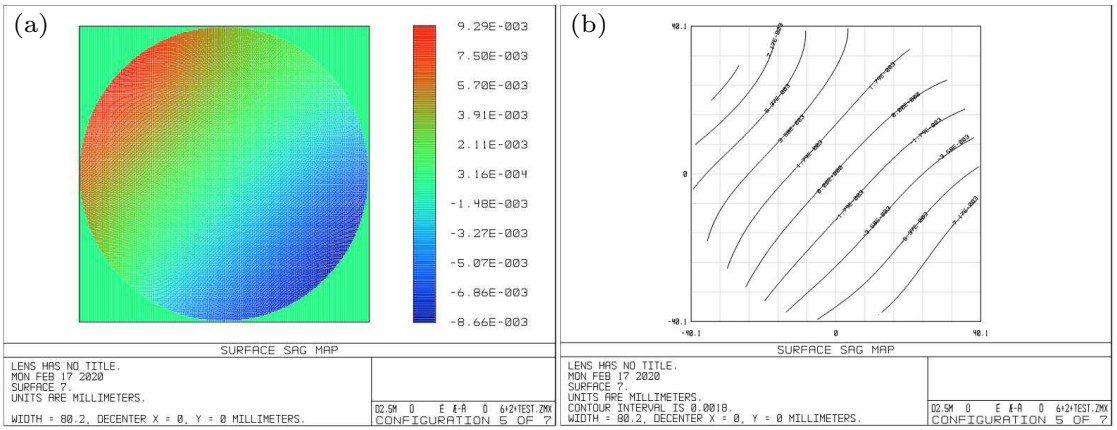


Fig. 10. Surface shape parameters of controller K: (a) exit pupil surface, (b) exit pupil surface contour.

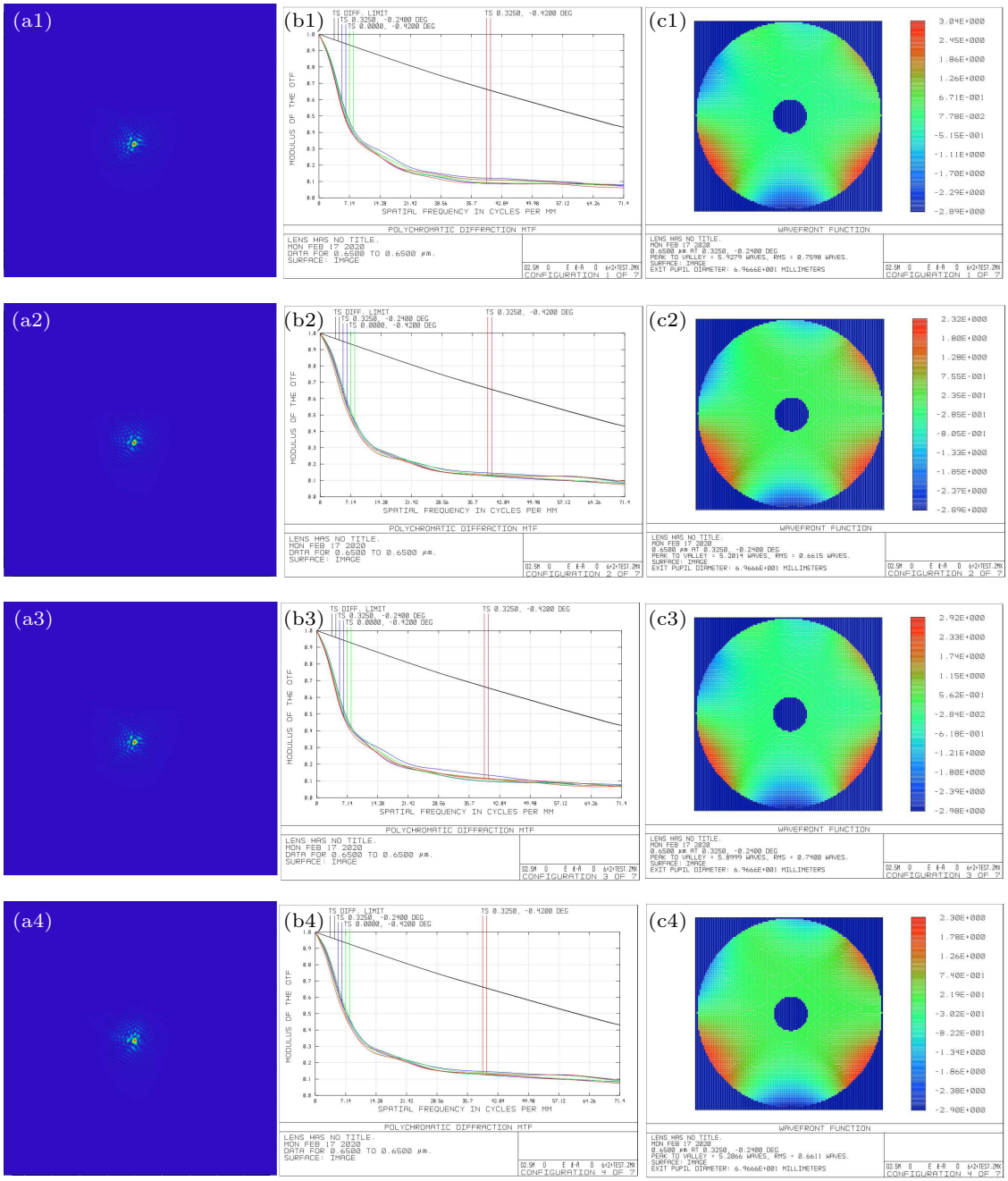


Fig. 11. High robustness design results of optical imaging system from config 1 to config 4. Panels (a1)–(a4) show PSF at common focal plane, panels (b1)–(b4) show MTF at common focal plane, panels (c1)–(c4) show wavefront diagram at the common focal plane.

3.2.2. Solution of pupil initial value

For the linear space-invariant incoherent imaging system, the image plane information collected by the k-th optical channel can be represented by the convolution operation of the object plane information and the PSF of the k-th optical channel. The phase difference is introduced by adding a known phase function to the generalized pupil function,[16] namely,

$$H_k(u) = |H_k(u)| \exp\{\mathrm{i}\,[\phi(u) + \theta_k(u)]\}, \tag{16}$$

where $\varphi(u)$ is the unknown wavefront aberration to be solved in the system, and $\theta_k(u)$ is the known phase difference function introduced by the k-th difference image plane. Here, $\varphi(u)$ is usually expressed in the form of the weighted sum of a series of Zernike polynomials, namely,

$$\phi(u) = \sum_{j=1}^{K} \alpha_j \phi_j(u), \tag{17}$$

where α_j represents the coefficient of the Zernike polynomial of the j-th term. Therefore, the aberration distribution in the system can be known by solving the coefficients of Zernike polynomials.

The objective function is constructed as follows based on the least square method:

$$L = -\sum_{k=1}^{K} \sum_{x} [d_k(x) - f * s_k(x)]^2. \tag{18}$$

Using PD technology to detect the wavefront is a large-scale, multivariable, nonlinear optimization process. When the objective function gets the minimum value, the phase information of the wavefront can be represented by the obtained Zernike coefficients by searching. L-BFGS algorithm is used to solve the objective function. The solved wavefront will be used as the initial value of pupil coding, which is the starting point of the next optimization.

3.3. Robust interval optimization of the optical system

The weight of each configuration is equal, and at the same time, the optimization of each weight structure is obtained by using the surface-changing formula of optical design and the least square method. Zernike system is used to describe the deformation parameters of pupil surface under different conditions.

The surface shape of the controller K obtained by solving the exit pupil surface is shown in Fig. 10.

It can be seen that the PSF shape, MTF curve and wavefront shape of the exit pupil in config 1–config 4 condition are very similar after the original optical system is optimized by high robustness design.[17–20] In order to verify the validity of the design optimization of high robustness, we perform the imaging simulation on the optical system with high robustness design, as shown in Fig. 12.

Table 4. Comparison of high robustness design imaging simulation results from config 1–config 4 by using SSIM.

Config	a	b	c	d
a	1	*	*	*
b	0.9709	1	*	*
c	0.9989	0.9715	1	*
d	0.9823	0.9768	0.9829	1

Note: * represents duplicate data.

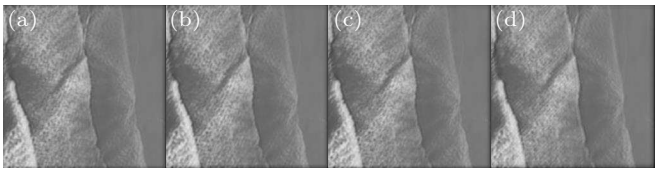


Fig. 12. High robustness design imaging simulation results of optical imaging system from config 1–config 4.

It can be seen that although the imaging quality of the optical system after the highly robust optimization design is reduced, the imaging results in the case of config 1–config 4 are very similar. And we use SSIM to calculate and compare the similarity of the high robustness design imaging simulation results from config 1–config 5, as shown in Table 4.

According to the calculation results of SSIM in Tables 3 and 4, it is shown that the optical system optimized by high robustness design has high imaging consistency in the face of errors caused by known external factors.

4. Result analysis and discussion

4.1. Generalization analysis of results

In the obtained results, the fifth configuration is added, which is not brought into the system. It is not used as the optimal disturbance source to participate in the optimal generation of the exit pupil surface, which is used to examine the correction ability of the results for other types of aberrations.

It can be seen that the PSF shape and MTF curve of the exit pupil of the config 5 structure are very similar to those of config 1–config 4 structure. Moreover, we simulate the imaging result on the optical system with the high robustness design of config 5, and compared them with the imaging simulation results of config 1–config 4, as shown in Fig. 14.

It can be seen that the simulation imaging results of config 5 are very similar to those of config 1–config 4. We use SSIM to calculate and compare the simulation imaging results of config 5 with the other four configs, as shown in Table 5.

Table 5. Comparison of high robustness design imaging simulation results from config 1–config 5 by using SSIM.

Config	a	b	c	d	e
a	1	*	*	*	*
b	0.9709	1	*	*	*
c	0.9989	0.9715	1	*	*
d	0.9823	0.9768	0.9829	1	*
e	0.9163	0.8805	0.9171	0.9225	1

Note: * represents duplicate data.

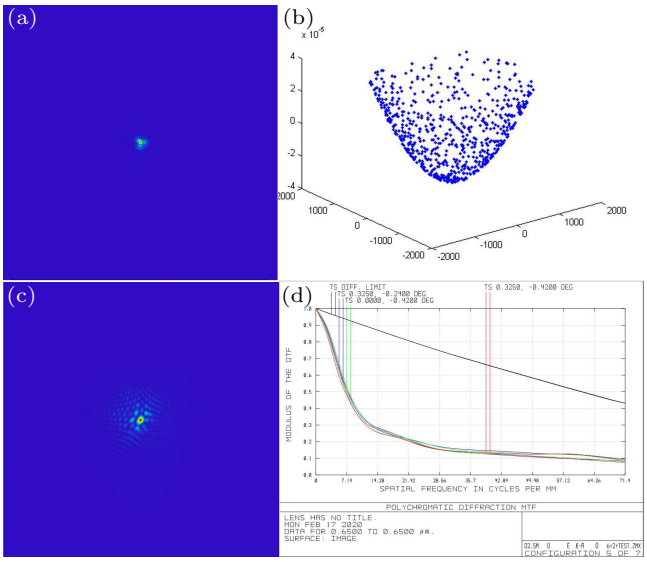


Fig. 13. Generalization analysis of high robustness design results of optical imaging system after adding the config 5. Panel (a) shows PSF directly produced by the aberration, panel (b) shows error term form at pupil position, panel (c) shows PSF 5 obtained by the aberration plus the exit pupil plane, and panel (d) shows MTF5 obtained by the aberration plus the exit pupil plane.

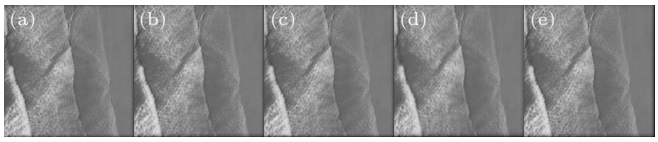


Fig. 14. High robustness design imaging simulation results of optical imaging system from config 1–config 5.

According to the results, there is a high consistency between the imaging result under config 5 and the imaging results under other conditions. It shows that the high robustness optimization method presented in this paper has the same control force on the error of the optical system caused by unknown external disturbances. The above methods have almost the same control ability for the aberrations not brought into the optimal design.

4.2. MTF robustness analysis

The MTF difference of the optical system before and after adding controller K under typical working conditions is quantitatively evaluated, and the results are as shown in Table 6.

Table 6. MTF robustness analysis before and after adding controller K to the optical imaging system.

Parameters	Before adding the controller K	After adding controller K
$\|\|\text{MTF1}-\text{MTF2}\|\|_2$	0.0908	0.0129
$\|\|\text{MTF1}-\text{MTF3}\|\|_2$	0.0157	0.0002
$\|\|\text{MTF1}-\text{MTF4}\|\|_2$	0.0760	0.0106
$\|\|\text{MTF1}-\text{MTF5}\|\|_2$	0.2214	0.0147

Note: The working condition1 is taken as the standard condition.

It can be seen from the above table that the stability of MTF in each working condition has been improved by one order of magnitude on average compared with the standard condition after adding the controller K in the optical system.

5. Conclusion

In this paper, the computational optical imaging method and fault-tolerant system control theory are used to establish a high-robustness imaging model of the optical system. Combined with the design of an actual large-aperture optical system, an optomechanical model and typical disturbance conditions are established to solve its robust interval, and the solution of its passive fault-tolerant controller K is given. Through the generalization and robustness analysis of the design results, it can be seen that this method can reduce the sensitivity of the computational imaging optical system to various disturbances, so as to ensure the imaging effect of the optical system under different working conditions is consistent. And it provides a feasible measure for reducing the requirements of optical imaging on processing, adjustment and environmental parameter accuracy.

References

[1] Dong D Y, Li Z L, Xue D L, Chen C Z and Zhang X J 2016 *Opt. Precis. Eng.* **24** 10
[2] Pang S W, Pan T, Mao Y L, Li X Y, Zhang M, Liu H Y, Wang Z Y and Zhu W H 2016 *Spacer. Environ. Eng.* **33** 305
[3] Li L, Wang D, Yang H B, Tan L Y and Sun Z L 2016 *Opt. Precis. Eng.* **24** 1677
[4] John M T 2010 *A study of image artifacts caused by structured mid-spatial frequency fabrication errors on optical surfaces*, Ph.D. dissertation (Tucson: The University of Arizona)
[5] Zhang Y J, Tang Y, Wang P, Li Y C, Zhu D L, Sun H, Chai L F and Chen B Y 2011 *Opto-Electron. Eng.* **38** 127
[6] Šiljak D D 1980 *Int. J. Control.* **31** 303
[7] Guan Y 2006 *Research on Satellite Attitude Control System based on Robust Fault-tolerant Control*, MS dissertation (Harbin: Harbin Institute of Technology) (in Chinese)
[8] Perry J W 1943 *Proc. Phys. Soc.* **55** 257
[9] Gray D S 1948 *J. Opt. Soc. Am.* **38** 542
[10] Johnston J D, Howard J M, Mosier G E, Parrish K A, McGinnis M A, Bluth A M, Kim K and Ha K Q 2004 *Optical, Infrared, and Millimeter Space Telescopes* (USA: SPIE-Int) p. 600
[11] Liu G 2019 *Research of the key technologies on active-thermal optics for the space camera based on structural-thermal-optical integration*, Ph.D. dissertation (Beijing: University of Chinese Academy of Sciences) (in Chinese)
[12] Cho M K and Poczulp G A 1991 *Proc. SPIE-Int. Soc. Opt. Eng.* **1532** 137
[13] Forman S E and Sultana J A 1990 *Advances in Optical Structure Systems* (USA: SPIE-Int) p. 65
[14] Gureyev T E, Roberts A and Nugent K A 1995 *J. Opt. Soc. Am. A* **12** 1932
[15] Prata A and Rusch W V T 1989 *Appl. Opt.* **28** 749
[16] Fisher R A 1983 *Opt. Lett.* **8** 611
[17] Huang W W, Zhao T Y, Zhang W Z and Yu F H 2007 *Opt. Instrum.* **29** 17
[18] Feng L T, Meng J H, Dun X and Tao Y 2011 *Infrared Laser Eng.* **40** 83
[19] Chen S Q, Fan Z G, Xu Z G, Zuo B J, Wang S and Xiao H S 2011 *Opt. Lett.* **36** 3021
[20] Gonzalo M, Amritpal S, Mathias A, David H, Andrew W and Andrew R H 2009 *Opt. Express* **17** 21118